Sustainable Energy & Fuels

Impact of ammonia decomposition reaction over anode on direct ammonia-fueled protonic ceramic fuel cells

Journal:	*Sustainable Energy & Fuels*
Manuscript ID	SE-ART-06-2020-000841.R2
Article Type:	Paper
Date Submitted by the Author:	06-Aug-2020
Complete List of Authors:	Miyazaki, Kazunari; Kyoto University Muroyama, Hiroki; Kyoto University, Matsui, Toshiaki; Kyoto University, Department of Energy and Hydrocarbon Chemistry, Graduate School of Engineering Eguchi, Koichi; Kyoto University, Department of Energy and Hydrocarbon Chemistry

ARTICLE

Impact of ammonia decomposition reaction over anode on direct ammonia-fueled protonic ceramic fuel cells

Received 00th January 20xx,
Accepted 00th January 20xx

DOI: 10.1039/x0xx00000x

Kazunari Miyazaki, Hiroki Muroyama, Toshiaki Matsui* and Koichi Eguchi*

Ammonia has been considered as a promising alternative energy carrier due to its high hydrogen content and lack of carbon. Since ammonia readily decomposes into hydrogen and nitrogen at high temperatures, it can be used as a fuel for solid oxide fuel cells (SOFCs). In this work, the effect of the ammonia decomposition reaction over an anode on the performance of direct ammonia-fueled SOFCs was evaluated by electrochemical measurements and catalytic activity tests. A Ni–$BaCe_{0.4}Zr_{0.4}Y_{0.2}O_{3-\delta}$ cermet with excellent catalytic activity for ammonia decomposition was employed as the anode material. Impedance analyses revealed that the total cell resistance strongly depended on the ammonia fuel supply conditions. Particularly, the polarization resistance, which was attributed to a mass transfer process in the anode, increased at high ammonia concentrations and flow rates. On the other hand, in the catalytic activity tests, the conversion of ammonia over the cermet decreased under such fuel supply conditions. Hence, it was concluded that the performance of direct ammonia-fueled SOFCs significantly depended on the ammonia conversion over the anode. Additionally, a considerable reduction in the anode temperature as a result of endothermic ammonia decomposition reaction was confirmed.

Introduction

Fuel cells are considered as some of the most promising energy devices. Unlike existing fossil fuel-based power plants, fuel cells can generate electricity without the limitation of the Carnot efficiency. Thus, a considerable reduction in the carbon dioxide emissions is expected for fuel cells. Notably, if only hydrogen and oxygen are chosen as the fuel and oxidant, respectively, water is obtained as the sole product of power generation by fuel cells. At present, hydrogen is produced by hydrocarbon reforming processes; however, it is known that carbon-free electricity supply can be realized by using hydrogen produced from renewable energy sources. Hence, numerous studies on the development of fuel cells and efficient production of hydrogen are currently ongoing around the world. Nevertheless, the costs of hydrogen storage and transportation significantly limit the implementation of hydrogen economy. Moreover, the gas exhibits low volumetric density and a boiling point of –253 ºC at ambient pressure. Consequently, non-hazardous hydrogen-containing compounds such as alcohols, methylcyclohexane, and ammonia have been proposed as hydrogen carriers.[1–6] Dehydrogenation of these compounds results in on-site hydrogen generation. Particularly, ammonia has attracted considerable attention due to its various advantages.[6–8] Firstly ammonia endothermically decomposes into hydrogen and nitrogen according to the following equation (eq. 1):

$$NH_3 \rightarrow 3/2\ H_2 + 1/2\ N_2 \quad \Delta H^o = +46\ \text{kJ mol}^{-1}\ (\text{at } 25\ ^oC) \qquad (1)$$

Importantly, since the compound is not composed of any carbon atoms, there is no possibility of carbon dioxide emissions upon the decomposition reaction. This unique feature is especially advantageous for reducing the atmospheric greenhouse gas concentrations. Secondly, ammonia is more easily liquefied than hydrogen because of its relatively high boiling point of –33 ºC at ambient pressure. Furthermore, since ammonia has already been extensively utilized as a starting material for the production of various fertilizers and chemicals, the additional capital investment is reduced.

Based on a thermodynamic calculation, the conversion of ammonia during a decomposition reaction (eq. 1) is over 99% above 400 ºC. To promote this reaction, different efficient catalysts based on Ru and Ni have been developed.[9–13] By employing these catalysts, hydrogen can be produced on-site. In addition, in solid oxide fuel cells (SOFCs) operating at high temperatures of 600–1000 ºC, ammonia can be used directly as a fuel. In such systems, the heat from the power generation of SOFCs is efficiently utilized for the endothermic decomposition of ammonia. Since in direct ammonia-fueled SOFCs the hydrogen produced via ammonia decomposition over an anode reacts with oxide ions, high ammonia decomposition activity is essential for anode materials. A number of studies have reported utilizing various nickel-based cermet anodes for ammonia decomposition. For instance, Ma et al. employed a conventional SOFC anode material, specifically Ni–yttria-stabilized zirconia (Ni–YSZ), in direct ammonia-fueled SOFCs and reported high cell performance, which was comparable with that of hydrogen fuel at 650–850 ºC.[14] Moreover, Meng et al. fabricated an anode-supported cell of Ni–samarium-doped ceria (Ni–SDC)|SDC|$Ba_{0.5}Sr_{0.5}Co_{0.8}Fe_{0.2}O_{3-\delta}$. The system achieved remarkably high performance of 1190 mW cm^{-2} at 650 ºC.[15] Although both studies successfully demonstrated power generation using ammonia as the fuel, the effects of ammonia decomposition over the anodes on the cell performance were not fully elucidated. Molouk et al. investigated the effect of ammonia fuel flow rate on the cell performance using a Ni–YSZ anode.[16] They determined a direct correlation between the catalytic activity of an anode for ammonia decomposition and the cell performance. It is particularly noteworthy that the performance

Department of Energy and Hydrocarbon Chemistry, Graduate School of Engineering, Kyoto University, Nishikyo-ku, Kyoto 615-8510, Japan. E-mail: eguchi@scl.kyoto-u.ac.jp; matsui@elech.kuic.kyoto-u.ac.jp

of ammonia-fueled SOFCs decreased at reduced temperatures due to the lack of ammonia decomposition activity of conventional cermets. On the other hand, Yang et al. developed a Ni–$BaCe_{0.75}Y_{0.25}O_{3-\delta}$ cermet exhibiting high activity for ammonia decomposition.[17] Compared with cells employing Ni–YSZ and Ni–SDC anodes, a reduction in the anode overpotential was achieved for direct ammonia-fueled SOFCs. We previously found that a Ni–$Ba(Zr,Y)O_{3-\delta}$ cermet displayed higher catalytic activity for ammonia decomposition than Ni–$BaCe_{0.75}Y_{0.25}O_{3-\delta}$.[18] Furthermore, a single cell employing a Ni–$Ba(Zr,Y)O_{3-\delta}$ anode, i.e., Ni–$BaZr_{0.8}Y_{0.2}O_{3-\delta}$|$BaZr_{0.8}Y_{0.2}O_{3-\delta}$|Pt, showed high performance when the ammonia fuel was fed at 600–700 ºC. Notably, the performance of the developed cell was comparable to that of a hydrogen fuel cell. Nonetheless, considering electrical conductivity, $BaZr_{0.8}Y_{0.2}O_{3-\delta}$ is inferior to $Ba(Ce,Y)O_{3-\delta}$. Specifically, the total electrical conductivities of $BaZr_{0.8}Y_{0.2}O_{3-\delta}$ and $BaCe_{0.8}Y_{0.2}O_{3-\delta}$ at 600 ºC in 3% humidified hydrogen are 2.7×10^{-3} S cm^{-1} and 1.0×10^{-2} S cm^{-1}, respectively.[19] To improve the proton conductivity of $BaZr_{0.8}Y_{0.2}O_{3-\delta}$, substitution of cerium for zirconium is effective. It has been reported that the composition of $BaCe_{0.4}Zr_{0.4}Y_{0.2}O_{3-\delta}$ (BCZY) is the optimum choice to achieve compatibility of proton conductivity and chemical stability.[20] Thus, in this study, the ammonia decomposition activity of a Ni–BCZY cermet was briefly evaluated. Subsequently, its applicability as an anode in direct ammonia-fueled SOFCs was assessed. To elucidate the effects of ammonia decomposition over an anode on the cell performance, the ammonia fuel was directly supplied under various conditions.

Experimental

Sample preparation

The $BaCe_{0.4}Zr_{0.4}Y_{0.2}O_{3-\delta}$ (BCZY) and $BaCe_{0.8}Y_{0.2}O_{3-\delta}$ (BCY20) powders were prepared by the citric acid complex method. Stoichiometric amounts of $Ba(NO_3)_2$ (Wako Pure Chemical Industries, Ltd.), $Ce(NO_3)_3{\cdot}6H_2O$ (Wako Pure Chemical Industries, Ltd.), $ZrO(NO_3)_2{\cdot}2H_2O$ (Wako Pure Chemical Industries, Ltd.), and $Y(NO_3)_3{\cdot}6H_2O$ (Sigma-Aldrich, Co.) were dissolved in deionized water. Subsequently, citric acid monohydrate (Wako Pure Chemical Industries, Ltd.) was added into the aqueous solution at a molar ratio of citric acid:total metal cations of 1.5:1. A 28% aqueous ammonia solution (Wako Pure Chemical Industries, Ltd.) was then added to adjust the pH to 8.0. The resultant solution was heated at 80 ºC using a hot plate until forming a transparent gel. The gel was subsequently fired at 350 ºC to cause auto-ignition. Finally, the resultant powder was calcined at 1100 ºC (BCY20) and 1200 ºC (BCZY) for 5 h in air.

The Ni–BCZY cermet for ammonia decomposition tests was prepared by physical mixing of NiO and BCZY. Following ball-milling of the NiO (Wako Pure Chemical Industries, Ltd.) and BCZY powders at the weight ratio of 60:40 overnight, the mixture was calcined at 1400 ºC for 5 h in air. For comparison, the conventional SOFC cermets, specifically Ni–YSZ and Ni–gadolinium-doped ceria (Ni–GDC), were prepared in the same manner using 8 mol% yttria-stabilized zirconia (Tosoh Co.) and 10 mol% gadolinium-doped ceria (Shin-Etsu Chemical Co., Ltd), respectively.

The phases of the prepared samples were identified by X-ray diffraction (XRD) analysis using Ultima IV X-ray diffractometer (Rigaku) with Cu Kα radiation. The specific surface areas of the cermets after reduction in a hydrogen atmosphere at 600 ºC were measured by the Brunauer–Emmett–Teller (BET) method with N_2 adsorption (Bellsorp-miniII, BEL Japan). As pretreatment, the cermet was heated at 300 ºC for 1 h in a vacuum.

Catalytic activity test for ammonia decomposition

The catalytic activity of the cermets for ammonia decomposition was evaluated using a fixed bed reactor. 300 mg of each sample was placed between silica wool layers in a quartz tube. Prior to the activity test, the samples were reduced at 600 ºC for 2 h under the supply of 50% H_2–50% Ar at a flow rate of 80 mL min^{-1}. Following reduction, the temperature was decreased to 350 ºC in an argon atmosphere. Subsequently, ammonia was supplied to the cermets at a flow rate of 30 mL min^{-1}. The conversion of ammonia over cermets was evaluated at 350–750 ºC. The unreacted ammonia in the gas outlet was removed by diluted sulfuric acid and the flow rate of the hydrogen and nitrogen gas mixture was measured utilizing a film flowmeter (HORIBA STEC). The ammonia conversion was calculated using eq. (2). It was assumed that the decomposition of ammonia into hydrogen and nitrogen occurred at a ratio of 3:1 (eq. (1)).

$$\text{Ammonia conversion (\%)} = (F_{out}/2F_{in}) \times 100, \quad (2)$$

where F_{in} and F_{out} indicate the flow rate of inlet ammonia gas and outlet H_2–N_2 gas mixture, respectively.

Furthermore, the ammonia decomposition behavior in the presence of hydrogen was evaluated at 500 ºC. It was previously reported that the ammonia decomposition rate depended on partial pressures of ammonia and hydrogen as follows;[21–23]

$$r_{NH3} = kP_{NH3}{}^{\alpha}P_{H2}{}^{\beta}, \quad (3)$$

where r_{NH3} is the reaction rate for ammonia decomposition, k denotes the rate constant, P_{NH3} and P_{H2} indicate the partial pressures of ammonia and hydrogen, while α and β denote the reaction order of ammonia and hydrogen, respectively. In the conducted test, the NH_3–H_2–Ar gas mixture was supplied at a total flow rate of 50 mL min^{-1}. The hydrogen concentration was varied from 15% to 30% under the fixed ammonia concentration of 30%.

Moreover, the ammonia decomposition over the Ni–BCZY cermet was investigated with varying the ammonia concentration and flow rate at a set temperature of 600 ºC. The change in the cermet temperature during ammonia decomposition was also measured using a thermocouple. The ammonia concentration was set to be the same as those in the following electrochemical measurements. The ammonia conversion was calculated using eq. (2).

Cell fabrication

The anode-supported single cell of Ni–BCZY|BCY20|BCY20–$La_{0.6}Sr_{0.4}Co_{0.2}Fe_{0.8}O_{3-\delta}$ (LSCF) was fabricated as follows. The NiO, BCZY, and polyvinyl butyral (mean molecular weight: 630, Wako Pure Chemical Industries, Ltd.) powders were ball-milled overnight at the weight ratio of 58:37:5. Subsequently, the mixed powder was uniaxially pressed at 50 MPa. The BCY20 electrolyte powder was then uniformly dispersed on the NiO–BCZY substrate, and the resulting bi-layer pellet was co-pressed at 50 MPa again. The obtained pellet was subjected to cold isostatic pressing at 300 MPa and then calcined at 1400 ºC for 5 h in air. To prepare the cathode, the LSCF (Kusaka Rare Metal Products Co., Ltd.) and BCY20 powders were ball-milled overnight at the weight ratio of 80:20. The resultant powder was then mixed with polyethylene glycol (mean molecular weight: 400, Wako Pure Chemical Industries, Ltd.) to obtain a cathode slurry. The slurry was subsequently screen-printed on the BCY20 electrolyte surface of the bi-layer pellet at the area of 0.636 cm^2, and calcined at 1150 ºC for 5 h in air. The

thickness of the electrolyte and anode was determined at 50–60 μm and 1.0 mm, respectively, while the diameter of the electrolyte was approximately 20 mm. The microstructure of the fabricated cell was analyzed by field-emission scanning electron microscopy (FE–SEM, NVision 40, Carl Zeiss-SIINT).

Electrochemical measurements

The anode-supported single cell was set between alumina tubes sealed using Pyrex glass rings and glass paste. As pretreatment, NiO–BCZY was reduced at 700 ºC in a hydrogen atmosphere for 1 h. Subsequently, the NH_3–Ar or H_2–Ar gas mixture and pure oxygen were supplied to the anode and cathode, respectively. The current–voltage characteristics and impedance spectra of the cell were measured at 550–700 ºC using the CellTest system (potentiostat/galvanostat 1470E and frequency response analyzer 1455, Solartron Analytical, UK). The impedance analysis was conducted in a frequency range of 1 MHz–0.1 Hz at an applied voltage amplitude of 30 mV.

Results and discussion

The nickel crystallite size and the BET surface area of the reduced cermets are summarized in Table 1. The crystallite size was estimated from the obtained XRD pattern using the Scherrer equation. The diffraction peak corresponding to the (111) plane of nickel was selected for the size estimation. Since all cermets were calcined at 1400 ºC prior to the reduction in a hydrogen atmosphere, the nickel crystallite sizes were relatively large. In addition, the surface areas of the cermets were significantly small. It is noteworthy that the grain size of nickel in Ni–BCZY was the largest among cermets studied.

We subsequently evaluated the ammonia decomposition activity of the cermets. The dependence of the ammonia conversion over cermets on the temperature is demonstrated in Fig. 1(a). For all cermets, the ammonia conversion was improved with an increase in temperature. For conventional SOFC anodes, i.e., Ni–YSZ and Ni–GDC, temperature as high as 750 ºC was required for the complete decomposition of ammonia. On the other hand, Ni–BCZY completely decomposed ammonia at 600 ºC despite the large grain size of nickel in the cermet. Since the cermet preparation method and the nickel loading amount in this study differ from those used in our previous work,[18,24] the catalytic activity of Ni–BCZY and Ni–Ba(Zr,Y)$O_{3-\delta}$ cannot be compared directly. The difference in the calcination temperature of the cermets was particularly large. Specifically, Ni–Ba(Zr,Y)$O_{3-\delta}$ was prepared by calcination at 700 ºC. Nevertheless, the temperature needed for complete decomposition of ammonia over Ni–BCZY was nearly the same as that required for decomposition over Ni–Ba(Zr,Y)$O_{3-\delta}$ at the identical space velocity. To understand the high catalytic activity of Ni–BCZY, the ammonia decomposition behavior in the presence of hydrogen was further evaluated at 500 ºC. The ammonia decomposition reaction over catalysts is typically inhibited by hydrogen due to its adsorption on the reaction sites, which is known as "hydrogen poisoning".[25–27] The extent of this phenomenon varies depending on the utilized catalyst materials. For example, Su et al. evaluated NiMgAl-layered double hydroxides as the ammonia decomposition catalysts.[28] It was confirmed that the ammonia conversion was enhanced as a result of the suppression of hydrogen poisoning by accelerating the hydrogen spillover from nickel to a catalyst support. Thus, high tolerance to hydrogen poisoning is one of the important factors for ammonia decomposition catalysts with high activity. Fig. 1(b) demonstrates the ammonia decomposition rate as a logarithmic function of partial hydrogen pressure. The reaction order of hydrogen (β) was calculated based on the slopes of the fitted lines using eq. (3). For all cermets, the ammonia decomposition rates exhibited a negative dependence on the partial hydrogen pressure. This indicated that as previously reported, the ammonia decomposition reactions over cermets were inhibited by hydrogen. However, the β value for Ni–BCZY was considerably larger than that for other cermets. In other words, the Ni–BCZY cermet showed high tolerance to hydrogen

Table 1 Nickel crystallite size and BET surface area of the cermets after reduction in 50% H_2–50% Ar

Sample	Ni crystallite size / nm [a]	BET surface area / $m^2\ g^{-1}$ [b]
Ni–BCZY	70.4	3.2
Ni–GDC	47.9	8.0
Ni–YSZ	45.0	5.5

[a] Estimated from XRD analysis
[b] Estimated from BET method

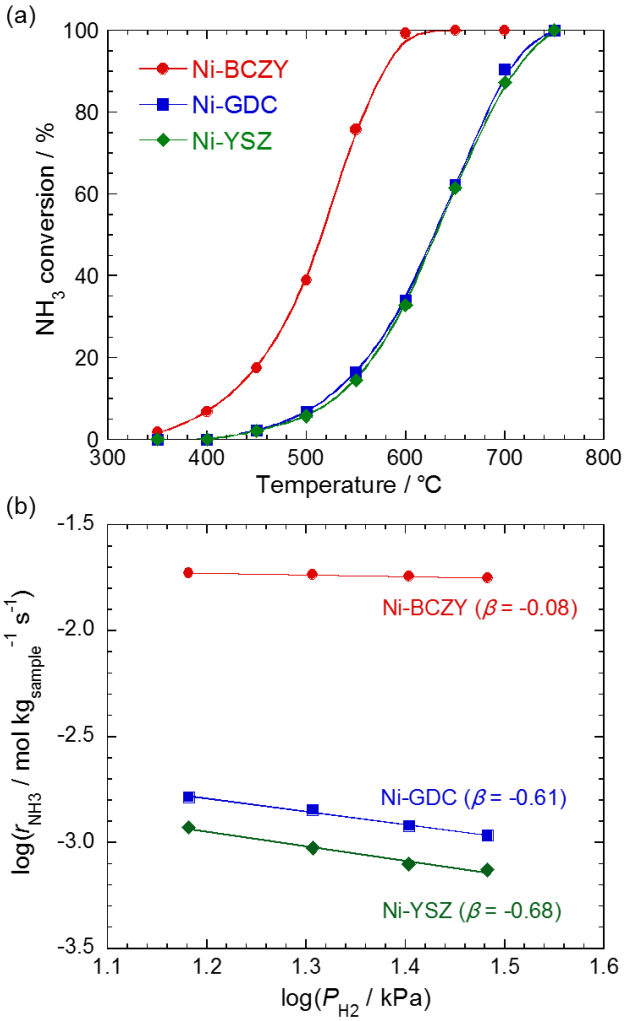

Fig. 1 (a) Ammonia conversion for ammonia decomposition over cermets. Reaction conditions: 100% NH_3, S.V. = 6,000 L kg^{-1} h^{-1}. (b) Ammonia decomposition rate as a function of partial pressure of hydrogen over cermets at 500 ºC, reaction conditions: x% H_2–30% NH_3–(70–x)% Ar (x = 15, 20, 25, 30), S.V. = 10,000 L kg^{-1} h^{-1}.

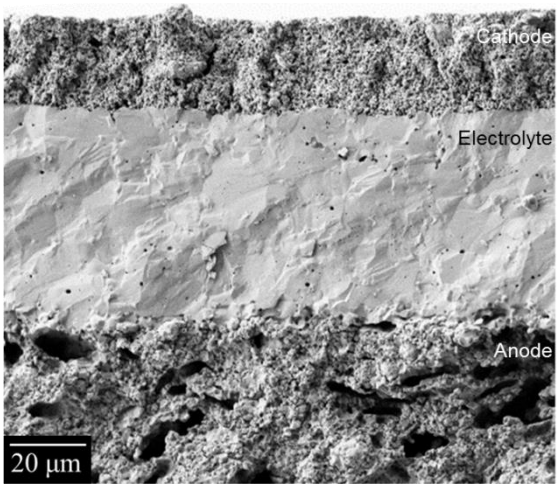

Fig. 2 Cross-sectional SEM image of the single cell, Ni–BCZY|BCY20|BCY20–LSCF.

poisoning. It was speculated that this property contributed to the notable ammonia decomposition activity of Ni–BCZY. In subsequent experiments, ammonia-fueled SOFCs employing a Ni–BCZY cermet anode were operated under various fuel supply conditions.

In the present study, we fabricated an anode-supported cell of Ni–BCZY|BCY20|BCY20–LSCF. To reduce the electrolyte resistance, BCY20 exhibiting high proton conductivity was used as the electrolyte. The cross-sectional SEM image of the cell is illustrated in Fig. 2. The BCY20 electrolyte was dense and free of cracks. Moreover, good adhesion of the electrodes to the BCY20 electrolyte was observed. However, since pore formers were not used during the cell fabrication, the porosity of the anode was low and the distribution of the pore sizes was not uniform. The power generation test was conducted with a supply of ammonia or hydrogen as the fuel and oxygen as the oxidant at 550–700 ºC. The ammonia gas composition in the ammonia fuel was controlled to obtain the same hydrogen concentration as that in the hydrogen fuel if ammonia decomposes completely into hydrogen and nitrogen. The current–voltage (*I–V*) and current–power (*I–P*) characteristics of the cell are shown in Fig. 3. The open circuit voltages (OCVs) of the cell were higher than 1.0 V under every condition as a result of the application of a gas-tight electrolyte. Nonetheless, the measured OCVs were relatively small due to a leak current in the electrolyte caused by the hole conduction of BCY20.[29] The contribution of the leak current becomes particularly large for the thinner electrolyte.[30,31] The maximum power density of the cell fueled with hydrogen reached 375 mW cm^{-2} at 700 ºC, despite the use of a non-optimized cell. Although this value was lower than the performance of PCFCs with a thin electrolyte layer fabricated by sophisticated deposition techniques,[32–34] it was sufficiently high to examine the effect of the ammonia supply conditions on the cell performance. The power generation test using an ammonia fuel revealed that the OCVs of the cell increased with decreasing temperature, which was consistent with the results obtained for a hydrogen fuel. This outcome supports the occurrence of a two-step reaction of ammonia over the anode; ammonia is decomposed into hydrogen and nitrogen over the anode, and then hydrogen is oxidized electrochemically. The high OCV values of the ammonia-fueled cell in the entire temperature range studied suggest excellent ammonia decomposition activity of the Ni–BCZY cermet. Furthermore, the power density for the ammonia fuel was close to that for the hydrogen fuel at every temperature. While the difference in the power density between fuels at 700 ºC seems to be larger than those at other temperatures, this is attributed to the difference in the local partial pressure of hydrogen in the anode; the hydrogen supply after ammonia

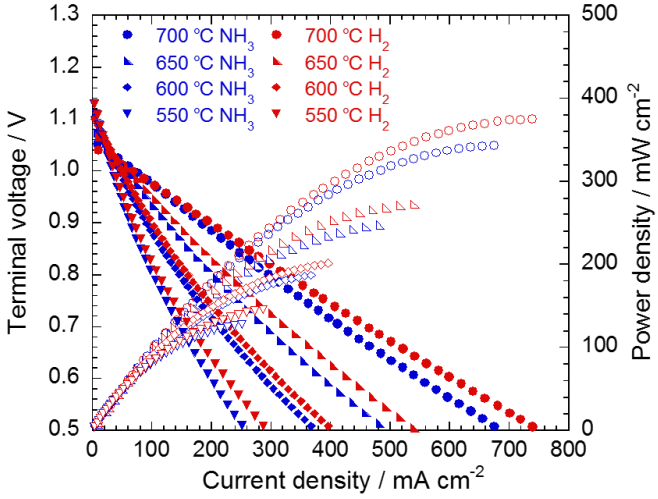

Fig. 3 *I–V* and *I–P* characteristics of the anode-supported single cell, namely Ni–BCZY|BCY20|BCY20–LSCF, at 550–700 ºC. Anode gas: 66.7% NH_3–33.3% Ar or 60.0% H_2–40.0% Ar, cathode gas: O_2.

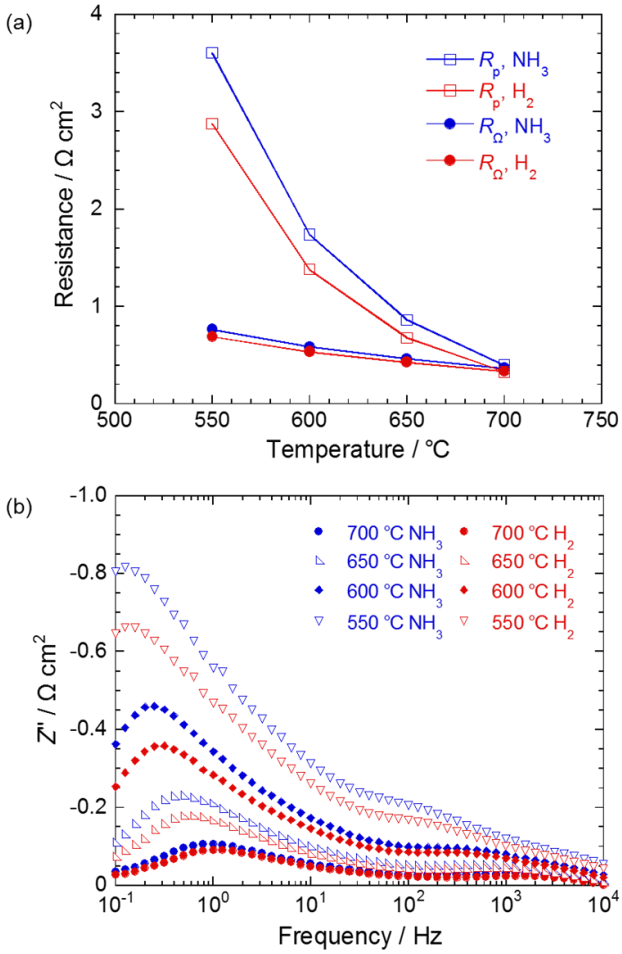

Fig. 4 (a) Ohmic and polarization resistance and (b) Bode plots of the impedance spectra of the anode-supported single cell (i.e., Ni–BCZY|BCY20|BCY20–LSCF) at 550–700 ºC. Anode gas: 66.7% NH_3–33.3% Ar or 60.0% H_2–40.0% Ar, cathode gas: O_2.

decomposition to the anode reaction site will be insufficient at high current densities. Anyway, it was determined that the Ni–BCZY cermet is a suitable anode for application in direct ammonia-fueled SOFCs. To elucidate the performance difference depending on the supplied fuels, the impedance analysis was performed under the open circuit condition. Fig. 4(a) shows the temperature dependence of the ohmic and polarization resistance (R_Ω and R_p, respectively) obtained from the impedance spectra of the cell supplied with ammonia or hydrogen at the same conditions as Fig. 3. The total cell resistance (i.e., $R_\Omega + R_p$) at each temperature reflected the slope of the *I*–*V* curves in the vicinity of the open circuit voltage. Notably, in every case, the resistance increased with decreasing temperature. However, the temperature dependence of each resistive component varied. The ohmic resistance increased gradually with declining temperature. The somewhat large ohmic resistance for the ammonia fuel was attributed to the reduction in the proton conductivity of the BCY20 electrolyte, which was a result of the cell temperature decrease caused by the endothermic ammonia decomposition over the anode. On the other hand, the polarization resistance rapidly increased at reduced temperatures. Consequently, the total resistance of the cell was dominated by the polarization resistance. The difference in the polarization resistance between both fuels expanded with falling temperature. Since the same cell and cathode gas were used in the conducted test, the difference mainly reflects the change in the anode resistance depending on the type of fuel. Although complete ammonia decomposition was achieved at temperatures above 600 ºC in the catalytic activity test, ammonia will not be completely decomposed in the anode chamber even at high temperatures due to the lack of porosity in the anode, as confirmed in our previous report.[18] Thus, below 650 ºC, the hydrogen concentration in the anode of an ammonia-fueled cell is expected to decrease to larger extent than that in the anode of a hydrogen-fueled cell. Fig. 4(b) shows the Bode plots of the impedance spectra of the cell at 550–700 ºC. Two distinct arcs were observed in the spectra at 10^{-1}–10^{2} and 10^{2}–10^{3} Hz. The resistance at a frequency of 10^{2}–10^{3} Hz, which was ascribed to the charge transfer process in the anode,[35] was relatively small, and its dependency on the fuel species was not significant. The polarization resistance was dominated by the resistance in the lower frequency range of 10^{-1}–10^{2} Hz. Notably, the resistance in this frequency range for ammonia was larger than that for hydrogen. Moreover, the difference in the resistance between the fuels increased with decreasing temperature. When the fuel was changed from hydrogen to ammonia, the peak shifted to a lower frequency. This indicated that the reaction rate of the elementary step corresponding to this frequency range decelerated in the case of the ammonia fuel. Generally, mass transfer resistance, e.g., for a diffusion of a gas and adsorbed species, emerges in relatively low frequency ranges in an impedance spectrum. Hence, it was concluded that the difference in the hydrogen diffusion process in the anode resulted in the variation in the polarization resistance under each fuel condition. This hypothesis is consistent with the decrease in the hydrogen concentration in ammonia-fueled SOFCs at reduced temperatures. Based on these impedance analyses, we confirmed the significant effect of ammonia decomposition over an anode on the cell performance. Ammonia decomposition over the Ni–BCZY cermet as well as the performance of ammonia-fueled SOFCs were subsequently comprehensively investigated under various ammonia supply conditions.

The dependency of the cell resistance on the ammonia concentration in the fuel was evaluated at 700 ºC. Fig. 5 displays the Nyquist plots of the impedance spectra of the cell supplied with ammonia fuels at various concentrations. The composition

Table 2 Composition of ammonia fuels

NH_3 concentration/ %	Flow rate / mL min^{-1}		
	NH_3	Ar	Total
25.0	20.0	60.0	80.0
42.9	30.0	40.0	70.0
66.7	40.0	20.0	60.0

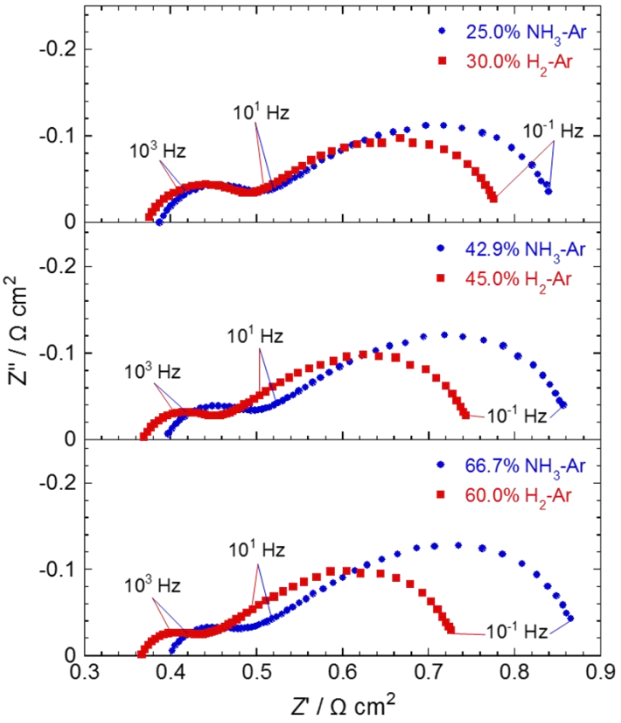

Fig. 5 Nyquist plot of the impedance spectra of the anode-supported single cell (i.e., Ni–BCZY|BCY20|BCY20–LSCF) supplied with fuel gases at various concentrations at 700 ºC. Anode gas: NH_3–Ar or H_2–Ar, cathode gas: O_2.

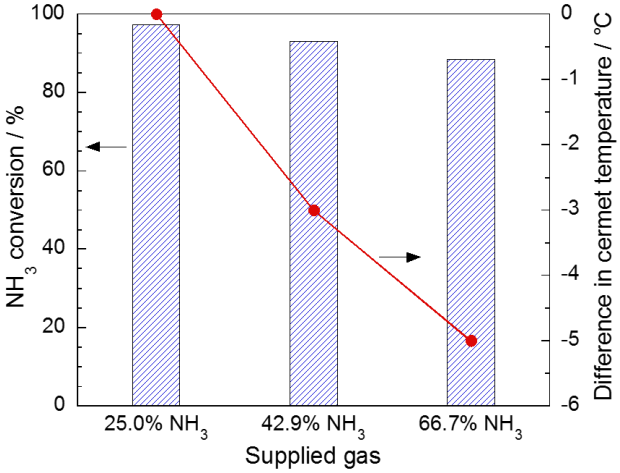

Fig. 6 Ammonia conversion for ammonia decomposition over the Ni–BCZY cermet and difference in the cermet temperature compared to that at the ammonia concentration of 25.0%. Reaction conditions: *x*% NH_3–Ar balance (*x* = 25.0, 42.9, and 66.7). Furnace temperature: 600 ºC.

of ammonia fuels was set according to the data shown in Table 2. The total gas flow rate upon complete ammonia decomposition was assumed at 100 mL min^{-1}. For comparison, the spectra for hydrogen fuels at the flow rate of 100 mL min^{-1} were also plotted. The hydrogen concentration in the hydrogen fuels was set to be the same as that in ammonia fuels after complete ammonia decomposition. For ammonia fuels, the total resistance gained with increasing ammonia concentration. In contrast, for hydrogen fuels, the total resistance reduced with increasing hydrogen concentration. Consequently, the difference in the total resistance for each fuel became larger at higher fuel concentrations. We subsequently focused on the evaluation of each resistive component. The ohmic resistance for ammonia fuels marginally increased with increasing ammonia concentration. However, in the case of hydrogen fuels, an opposite trend was observed. Moreover, the dependency of the polarization resistance of the cell on the ammonia concentration varied depending on the frequency range. The arcs in higher (> 10^2 Hz) and lower frequency ranges (10^{-1}–10^2 Hz) shrunk and expanded with increasing ammonia concentration, respectively. Considering that the polarization resistance in relatively high frequency ranges is typically attributed to the charge transfer step, the arc at above 10^2 Hz in the impedance spectrum was expected to contain the resistance for the electrochemical hydrogen oxidation. The impedance spectra obtained for hydrogen fuels revealed that the resistance in this range became smaller at high hydrogen concentrations. Moreover, the concentration of hydrogen produced by ammonia decomposition over the anode rises with increasing ammonia concentration. Thus, for ammonia fuels, the dependence of the polarization resistance on the fuel concentration in the higher frequency range was similar to that for hydrogen fuels. On the other hand, the resistance in the low frequency range, which corresponded to a mass transfer process, was reduced with increasing hydrogen concentration in hydrogen fuels. The decrease in the resistance at high hydrogen concentration was unsurprising. However, the resistance in the low frequency range enlarged for the cell supplied with high concentration of ammonia. Hence, for further analysis of the effect of ammonia concentration on the cell resistance, we conducted the catalytic activity test using a Ni–BCZY cermet under a supply of a NH_3–Ar gas mixture at the same gas composition as Fig. 5. Since nearly 100% ammonia conversion achieved for all gas compositions at 700 ºC, the test was performed at 600 ºC to determine the influence of the ammonia concentration on the decomposition behavior. The ammonia conversion over a Ni–BCZY cermet under the supply of different concentrations of ammonia is demonstrated in Fig. 6. The variation in the cermet temperature from that supplied with ammonia at a concentration of 25.0% was also plotted. Both values decreased with an increase in the ammonia concentration. Since ammonia decomposition is an endothermic process, the difference in the cermet temperature varied depending on the ammonia concentration, i.e., on the amount of ammonia decomposed over the cermet per unit time. This result confirmed that the cermet temperature was significantly affected by the ammonia concentration. In this test, the drop in the cermet temperature upon changing the ammonia concentration from 25.0% to 66.7% was determined at just 5 ºC. However, considering that the thermocouple was placed under silica wool, the actual cermet temperature could be lower than the measured one. Based on these results, we evaluated the impedance spectra shown in Fig. 5 again. Since the ammonia decomposition reaction reduced the temperature of the anode and electrolyte, the

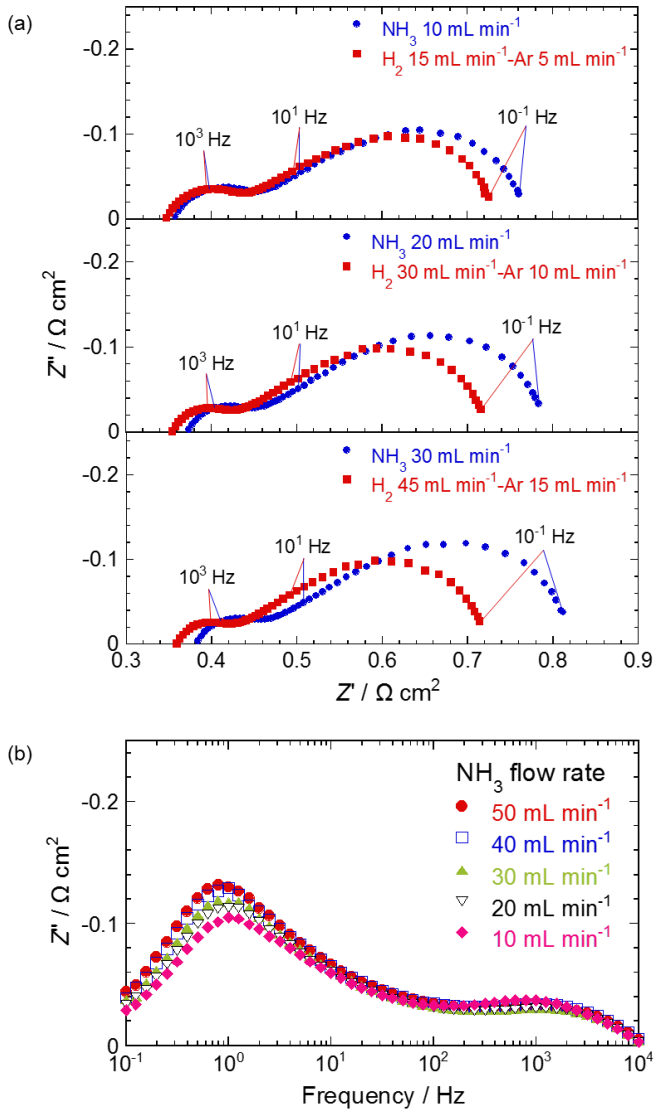

Fig. 7 (a) Nyquist and (b) Bode plots of the impedance spectra of the anode-supported single cell (i.e., Ni–BCZY|BCY20|BCY20–LSCF) supplied with fuel gases at various flow rates at 700 ºC. Anode gas: NH_3 or 75% H_2–25% Ar, cathode gas: O_2.

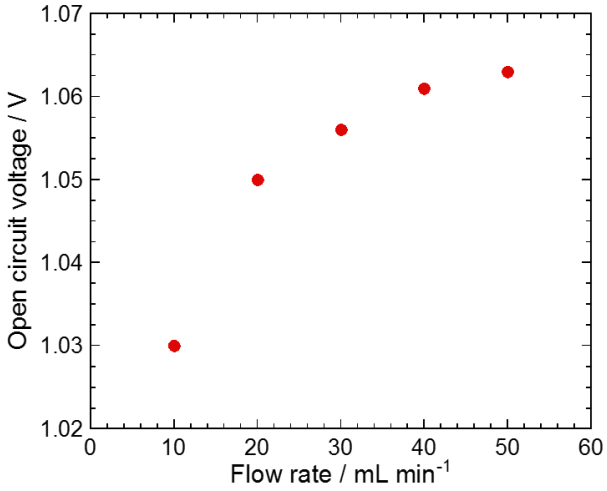

Fig. 8 Open circuit voltage of the anode-supported single cell (i.e., Ni–BCZY|BCY20|BCY20–LSCF) supplied with ammonia at various flow rates at 700 ºC. Anode gas: NH_3, cathode gas: O_2.

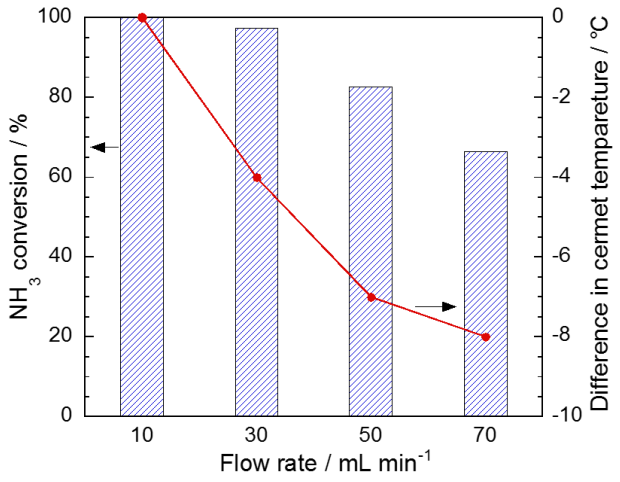

Fig. 9 Ammonia conversion for ammonia decomposition over the Ni–BCZY cermet and difference in the cermet temperature compared to that at the ammonia flow rate of 10 mL min^{-1}. Reaction conditions: 100% NH_3. Furnace temperature: 600 ºC.

electrical conductivities of BCZY and BCY20 decreased under the supply of ammonia at a high concentration. It was speculated that this was the reason for a slight increase in the ohmic resistance with increasing ammonia concentration. In addition, the gas flow rate in the vicinity of the electrochemical hydrogen oxidation reaction site decreased as a result of the reduction in the ammonia conversion. Since the flow rate of each ammonia fuel was set to be the same upon complete ammonia decomposition, the total flow rate of the reformed ammonia fuels became small at the low ammonia conversions. Consequently, increased polarization resistance in the low frequency range was observed at high concentrations of ammonia.

We then investigated the effect of the ammonia flow rate on the cell resistance at 700 ºC. In this measurement, pure ammonia was supplied to the anode. Fig. 7(a) demonstrates the Nyquist plots of the impedance spectra of the cell supplied with ammonia at various flow rates. The spectra for hydrogen fuels are also displayed. The spectral shape for hydrogen was nearly the same, regardless of the fuel flow rate. Conversely, in the case of ammonia fuels, a change in the shape of the spectra was noted. Both ohmic and polarization resistances increased with rising ammonia flow rate. As shown in the Bode plots for ammonia fuels in Fig. 7(b), the polarization resistance in the lower frequency range (10^{-1}–10^{2} Hz) was predominantly affected by the flow rate. Furthermore, as demonstrated in Fig. 8, the OCVs of the cell increased with increasing ammonia flow rate. As the flow rate of ammonia was the only difference in each condition, it was deciphered that the enhancement in OCVs was caused either by the increase in the hydrogen concentration at the anode or the decrease in the cell temperature. To further elucidate these results, the catalytic activity test was performed at 600 ºC under the same gas supply conditions as Fig. 7. Fig. 9 shows the conversion of ammonia over the Ni–BCZY cermet. Compared to the result at a flow rate of 10 mL min^{-1}, a drop in the cermet temperature at each ammonia flow rate was noted. It is evident that the decomposition of ammonia was significantly suppressed at high flow rates due to short contact time between the feeding gas and cermet. Hence, one of the reasons for the increase in the total resistance of the cell at high ammonia flow rates in Fig. 7(a) is the reduction in the hydrogen concentration at the anode. In addition, the cermet temperature was lessened at a high flow rate. Based on this result, we speculated that the falling cell temperature caused by the endothermic ammonia decomposition considerably affected the cell resistance. The specific variations in the arc width in the low frequency range of the impedance spectra can be explained by the reduction in the cell temperature as well as the decrease in the hydrogen concentration. It is well known that the effective gas diffusion coefficient (D_e) exhibits the following temperature dependency:[36,37]

$$D_e \propto T^{1.75}, \quad (4)$$

where T indicates the absolute temperature. According to this relation, the effect of the temperature change on the hydrogen diffusion in the anode is not significant. Hence, the decrease in the hydrogen concentration at the anode is a primary reason for the increase in the polarization resistance in the low frequency range. On the other hand, considering the outcomes of the catalytic activity tests, the variation in OCVs depending on the ammonia flow rate was primarily induced by the change in the cermet temperature. Although the difference in OCVs could also be attributed to the hole conduction in the BCY20 electrolyte, the present result implies a considerable reduction in the cell temperature as the key reason for this phenomenon.

Conclusions

The effect of ammonia decomposition over an anode on direct ammonia-fueled SOFCs was assessed under various fuel supply conditions. In this study, a Ni–BCZY cermet exhibiting excellent catalytic activity for ammonia decomposition was developed. It was established that the remarkable tolerance of the cermet to hydrogen poisoning was the main reason for high activity. The anode-supported cell of Ni–BCZY|BCY20|BCY20–LSCF fed with ammonia displayed high performance at temperatures in the range of 550–700 ºC. However, the total cell resistance for an ammonia fuel increased at reduced temperatures more severely than that for a hydrogen fuel. The polarization resistance attributed to a mass transfer process showed particularly large dependence on the fuel species. In addition, the resistance also increased under the supply of ammonia at higher concentrations and flow rates. In the catalytic activity test, the ammonia decomposition reaction over the Ni–BCZY cermet decelerated with increasing concentration and flow rate of ammonia. Based on the obtained results, it was concluded that the performance of direct ammonia-fueled SOFCs strongly depended on the ammonia conversion over the anode. Moreover, we found that the temperature of the Ni–BCZY cermet considerably dropped during the endothermic ammonia decomposition. Thus, the cell design considering the temperature distribution is an important factor for the long-term operation of direct ammonia-fueled SOFCs.

Conflicts of interest

There are no conflicts to declare.

Acknowledgements

This work was supported by Council for Science, Technology and Innovation (CSTI), Cross-ministerial Strategic Innovation Promotion Program (SIP), “energy carrier” (Funding agency: JST).

Notes and references

1 X. Zhang, N. He, L. Lin, Q. Zhu, G. Wang and H. Guo, *Catal. Sci. Technol.*, 2020, **10**, 1171–1181.
2 J. Yan, W. Wang, L. Miao, K. Wu, G. Chen, Y. Huang and Y. Yang, *Int. J. Hydrogen Energy*, 2018, **43**, 9343–9352.
3 T. Okanishi, Y. Katayama, R. Ito, H. Muroyama, T. Matsui and K. Eguchi, *Phys. Chem. Chem. Phys.*, 2016, **18**, 10109–10115.
4 M. Niermann, A. Beckendorff, M. Kaltschmitt and K. Bonhoff, *Int. J. Hydrogen Energy*, 2019, **44**, 6631–6654.
5 E. R. López, F. Dorado and A. de Lucas-Consuegra, *Appl. Catal. B Environ.*, 2019, **243**, 355–364.
6 R. Zhao, H. Xie, L. Chang, X. Zhang, X. Zhu, X. Tong, T. Wang, Y. Luo, P. Wei, Z. Wang and X. Sun, *EnergyChem*, 2019, **1**, 100011.
7 K. E. Lamb, M. D. Dolan and D. F. Kennedy, *Int. J. Hydrogen Energy*, 2019, **44**, 3580–3593.
8 M. Xue, Q. Wang, B. Le Lin and K. Tsunemi, *ACS Sustain. Chem. Eng.*, 2019, **7**, 12494–12500.
9 X. Ju, L. Liu, X. Zhang, J. Feng, T. He and P. Chen, *ChemCatChem*, 2019, **11**, 4161–4170.
10 Z. Hu, J. Mahin, S. Datta, T. E. Bell and L. Torrente-Murciano, *Top. Catal.*, 2019, **62**, 1169–1177.
11 X. C. Hu, X. P. Fu, W. W. Wang, X. Wang, K. Wu, R. Si, C. Ma, C. J. Jia and C. H. Yan, *Appl. Catal. B Environ.*, 2020, **268**, 118424.
12 S. Henpraserttae, S. Charojrochkul, W. Klysubun, L. Lawtrakul and P. Toochinda, *Catal. Letters*, 2018, **148**, 1775–1783.
13 K. Okura, K. Miyazaki, H. Muroyama, T. Matsui and K. Eguchi, *RSC Adv.*, 2018, **8**, 32102–32110.
14 Q. Ma, J. Ma, S. Zhou, R. Yan, J. Gao and G. Meng, *J. Power Sources*, 2007, **164**, 86–89.
15 G. Meng, C. Jiang, J. Ma, Q. Ma and X. Liu, *J. Power Sources*, 2007, **173**, 189–193.
16 A. F. S. Molouk, T. Okanishi, H. Muroyama, T. Matsui and K. Eguchi, *J. Electrochem. Soc.*, 2015, **162**, F1268–F1274.
17 J. Yang, A. F. S. Molouk, T. Okanishi, H. Muroyama, T. Matsui and K. Eguchi, *ACS Appl. Mater. Interfaces*, 2015, **7**, 7406–7412.
18 K. Miyazaki, T. Okanishi, H. Muroyama, T. Matsui and K. Eguchi, *J. Power Sources*, 2017, **365**, 148–154.
19 D. A. Medvedev, J. G. Lyagaeva, E. V. Gorbova, A. K. Demin and P. Tsiakaras, *Prog. Mater. Sci.*, 2016, **75**, 38–79.
20 P. Sawant, S. Varma, B. N. Wani and S. R. Bharadwaj, *Int. J. Hydrogen Energy*, 2012, **37**, 3848–3856.
21 K. Okura, T. Okanishi, H. Muroyama, T. Matsui and K. Eguchi, *ChemCatChem*, 2016, **8**, 2988–2995.
22 Z. Wang, Z. Cai and Z. Wei, *ACS Sustain. Chem. Eng.*, 2019, **7**, 8226–8235.
23 S. Armenise, F. Cazaña, A. Monzón and E. García-Bordejé, *Fuel*, 2018, **233**, 851–859.
24 K. Okura, T. Okanishi, H. Muroyama, T. Matsui and K. Eguchi, *Appl. Catal. A Gen.*, 2015, **505**, 77–85.
25 A. Srifa, K. Okura, T. Okanishi, H. Muroyama, T. Matsui and K. Eguchi, *Appl. Catal. B Environ.*, 2017, **218**, 1–8.
26 K. Kishida, M. Kitano, Y. Inoue, M. Sasase, T. Nakao, T. Tada, H. Abe, Y. Niwa, T. Yokoyama, M. Hara and H. Hosono, *Chem. - A Eur. J.*, 2018, **24**, 7976–7984.
27 L. Li, W. Chu, C. Ding, X. Xi, R. Jiang and J. Yan, *Int. J. Hydrogen Energy*, 2017, **42**, 30630–30638.
28 Q. Su, L. Gu, Y. Yao, J. Zhao, W. Ji, W. Ding and C. T. Au, *Appl. Catal. B Environ.*, 2017, **201**, 451–460.
29 Á. Triviño-Peláez, D. Pérez-Coll and G. C. Mather, *Acta Mater.*, 2019, **167**, 12–22.
30 K. L. Duncan, K. T. Lee and E. D. Wachsman, *J. Power Sources*, 2011, **196**, 2445–2451.
31 T. Nakamura, S. Mizunuma, Y. Kimura, Y. Mikami, K. Yamauchi, T. Kuroha, N. Taniguchi, Y. Tsuji, Y. Okuyama and K. Amezawa, *J. Mater. Chem. A*, 2018, **6**, 15771–15780.
32 K. Bae, D. Y. Jang, H. J. Choi, D. Kim, J. Hong, B. K. Kim, J. H. Lee, J. W. Son and J. H. Shim, *Nat. Commun.*, 2017, **8**, 1–9.
33 Y. Aoki, S. Kobayashi, T. Yamaguchi, E. Tsuji, H. Habazaki, K. Yashiro, T. Kawada and T. Ohtsuka, *J. Phys. Chem. C*, 2016, **120**, 15976–15985.
34 D. Konwar, B. J. Park, P. Basumatary and H. H. Yoon, *J. Power Sources*, 2017, **353**, 254–259.
35 S. Sun, O. Awadallah and Z. Cheng, *J. Power Sources*, 2018, **378**, 255–263.
36 T. Matsui, H. Fujii, A. Ozaki, T. Takeuchi, R. Kikuchi and K. Eguchi, *J. Electrochem. Soc.*, 2007, **154**, B1237–B1241.
37 I. Khazaee and A. Rava, *Energy*, 2017, **119**, 235–244.

Graphical abstract

The relation between a performance of direct ammonia-fueled SOFCs and an ammonia decomposition behavior over an anode was studied under various ammonia supply conditions.